Energies **2015**, *8*, 9719-9730; doi:10.3390/en8099719

OPEN ACCESS

energies

ISSN 1996-1073

www.mdpi.com/journal/energies

Article

Determining the Frequency for Load-Independent Output Current in Three-Coil Wireless Power Transfer System

Longzhao Sun *, Houjun Tang and Yingyi Zhang

Department of Electrical Engineering, Shanghai Jiao Tong University, Shanghai 200240, China; E-Mails: hjtang@sjtu.edu.cn (H.T.); Rachel0810@sjtu.edu.cn (Y.Z.)

* Author to whom correspondence should be addressed; E-Mail: sunlongzhao@sjtu.edu.cn; Tel.: +86-150-0086-2302.

Academic Editor: K. T. Chau

Received: 29 July 2015 / Accepted: 31 August 2015 / Published: 9 September 2015

Abstract: Conditions for load-independent output voltage or current in two-coil wireless power transfer (WPT) systems have been studied. However, analysis of load-independent output current in three-coil WPT system is still lacking in previous studies. This paper investigates the output current characteristics of a three-coil WPT system against load variations, and determines the operating frequency to achieve a constant output current. First, a three-coil WPT system is modeled by circuit theory, and the analytical expression of the root-mean-square of the output current is derived. By substituting the coupling coefficients, the quality factor, and the resonant frequency of each coil, we propose a method of calculating the frequency for load-independent output current in a three-coil WPT system, which indicates that there are two frequencies that can achieve load-independent output current. Experiments are conducted to validate these analytical results.

Keywords: three-coil; wireless power transfer (WPT); frequency; load-independent output current

1. Introduction

Nowadays, with its considerable potential for practical applications, wireless power transfer (WPT) technology is gaining much attention from researchers. WPT system can deliver electrical energy from

a power source to a load via varying magnetic fields, and the transmission power level ranges from a few milliwatts to several hundred kilowatts.

There are many benefits that make this technique particularly attractive, such as the electrical and mechanical isolation, the decrease in maintenance costs, and the potential for use in harsh environments. Therefore, WPT can be used for wireless battery charging for implantable biomedical devices [1–4] and portable electronics [5–7]. Moreover, even electric vehicles (or roadway-powered electric vehicles) can be wirelessly powered [8–11].

In terms of practical applications, most of the circuits and systems require constant source supply for stable operation; therefore, a relatively constant output in WPT system is desired regardless of load variations.

In two-coil WPT systems, there have been many efforts [1,2,12–17] to regulate the output voltage under varying couplings and loads. [12–15] exhibited relatively constant output voltage under coupling variations. However, the variation of output voltage is relatively high, and the distance range for constant output is limited. In addition, the effect of load variations on output voltage is not discussed. In [1], using the transformer model, the voltage transfer function was obtained; an operating frequency corresponding to a particular coupling coefficient could be found, for which the voltage transfer function was irrelevant to load. In [2], the output voltage was insensitive to loading variations if the operating frequency was adjusted according to coupling variations, and a parallel-resonant class-D oscillator transmitter was developed to track this optimal operating frequency. In [16], a design and optimization method was proposed to achieve a better overall efficiency and good output voltage controllability in a WPT system. For both the secondary series- and parallel-compensations in two-coil WPT, by calculating the partial derivative of the voltage gain with respect to the load, [17] analyzed the frequencies that could provide a constant voltage gain despite load variations.

However, in some charging applications, a load-independent output current is more desirable. For example, a constant output current is preferred for driving an LED to have stable luminance, or multistep constant current of a charging profile to charge a battery pack for electric vehicles. An extra current regulator stage, which results in extra power loss, is needed if the WPT system outputs as a voltage source. In [18], operating frequencies for maximal efficiency and load-independent output current in two-coil WPT are explored. Moreover, the dual circuits of the secondary series- and parallel-compensated WPT have been studied. It is found that the trend of the output current of a series-compensated (parallel-compensated) WPT system studied in [18] replicates the trend of the output voltage of a parallel-compensated (series-compensated) WPT system in [17].

With increasing transmission distance in two-coil WPT, the performance of the two-coil WPT deteriorates. Adding a repeating coil, which receives the magnetic field from the transmitter and then relays the magnetic field to the receiver, enhances inductive coupling at longer distances. However, a detailed analysis of load-independent output current in such a three-coil WPT system is still lacking in previous studies.

In this study, a three-coil WPT system is investigated. To determine the operating frequency for the particular coupling coefficient—in this case, the output current remains constant despite changes in the load—we first substitute the coupling coefficients, the quality factor, and the resonant frequency of each coil into the expression of the root-mean-square (RMS) of the output current, and then the frequencies

that can provide load-independent output current in a three-coil WPT are found for the first time. To verify the results of this analysis, theoretical calculations and experiments are conducted.

2. Modeling

Figure 1 presents a photograph of a three-coil WPT system. The AC voltage source supplies power for the transmitting coil (TX). Through the inductive coupling between the coils, current can be induced in the receiving coil (RX), providing power for the load [19,20].

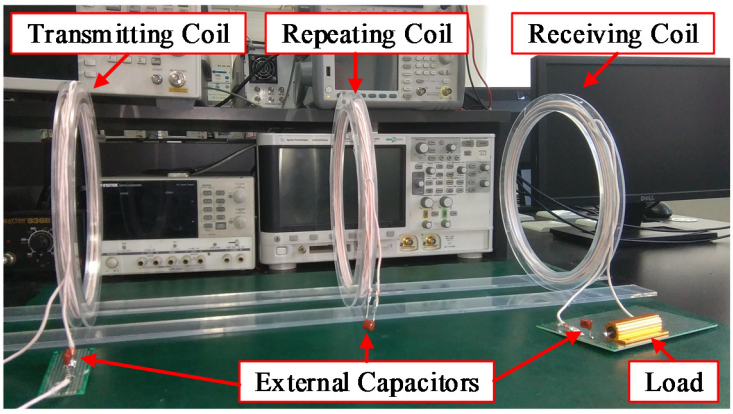

Figure 1. Photograph of a three-coil WPT system.

As shown in Figure 2, the WPT system can be modeled by circuit theory [21,22]. A constant AC voltage source V_{in} is used for the power supply, and R_L is the loading resistor. The TX, the repeating coil, and the RX are represented as a resistor-inductor-capacitor (RLC) circuit, and the inductive coupling between the coils is described by the mutual inductance. The parameters of the TX are denoted with subscript 1, the repeating coil with subscript 2, and the RX with subscript 3. L_i is the inductance of coil i ($i=1,2,3$), whose equivalent resistance is R_i, and external capacitor C_i is added to form a series-tuned topology. M_{12} and M_{23} are the mutual inductances between each two adjacent coils, and M_{13} is the mutual inductance between the TX and the RX.

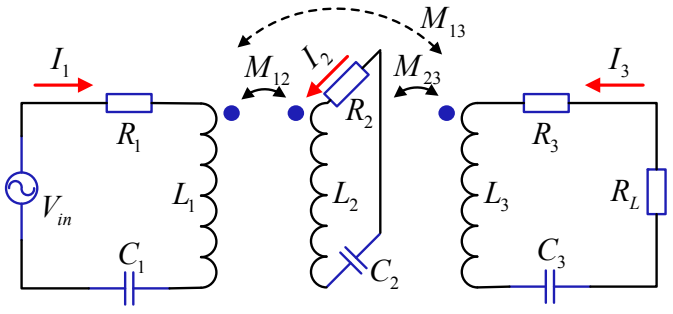

Figure 2. Equivalent circuit of the three-coil WPT system.

3. Frequency for Load-Independent Output Current in Three-Coil WPT

The Kirchhoff's voltage law (KVL) equations of the equivalent circuit in Figure 2 are:

$$\begin{bmatrix} R_1 + j\omega L_1 + \dfrac{1}{j\omega C_1} & j\omega M_{12} & j\omega M_{13} \\ j\omega M_{12} & R_2 + j\omega L_2 + \dfrac{1}{j\omega C_2} & j\omega M_{23} \\ j\omega M_{13} & j\omega M_{23} & R_3 + j\omega L_3 + \dfrac{1}{j\omega C_3} + R_L \end{bmatrix} \begin{bmatrix} \mathbf{I_1} \\ \mathbf{I_2} \\ \mathbf{I_3} \end{bmatrix} = \begin{bmatrix} \mathbf{V_{in}} \\ 0 \\ 0 \end{bmatrix} \quad (1)$$

where $\mathbf{I_i}$ is the current in the coil i ($i = 1, 2, 3$), $\mathbf{V_{in}}$ is the voltage source, and ω is the operating frequency.

In this study, bold letters are used to represent the phasors, and italic letters denote real numbers or RMS values of the phasors. For example, $\mathbf{I_1}$ is a current phasor, and I_1 is the RMS value of $\mathbf{I_1}$. For the given three-coil WPT system, the equivalent resistances of the coils are small enough to be omitted. For simplicity, the cross-coupling M_{13} is neglected in comparison to the coupling between adjacent coils M_{12} and M_{23}.

The expression of the output current $\mathbf{I_3}$ can be obtained by solving Equation (1). To facilitate the analysis, six factors are introduced: the coupling coefficients k_{12} and k_{23}, the quality factor Q, the resonant frequency ω_i ($i = 1, 2, 3$) of the coil i. These factors are, respectively, defined as:

$$k_{12} = M_{12}/\sqrt{L_1 L_2}, \quad k_{23} = M_{23}/\sqrt{L_2 L_3}, \quad Q = \omega_3 L/R_L, \quad \omega_i = 1/\sqrt{L_i C_i} \ (i = 1, 2, 3) \quad (2)$$

By substituting Equation (2) into the expression of $\mathbf{I_3}$, the RMS of $\mathbf{I_3}$ can be derived by:

$$I_3 = \frac{\sqrt{C_1 C_3}\, k_{12} k_{23} \omega^5 V_{in}}{\omega_1 \omega_2^2 \omega_3 \sqrt{\left(\frac{\omega^2}{\omega_1^2} + \frac{\omega^2}{\omega_2^2} + \frac{\omega^2}{\omega_3^2} - \frac{\left(1 - k_{12}^2\right)\omega^4}{\omega_1^2 \omega_2^2} - \frac{\left(1 - k_{23}^2\right)\omega^4}{\omega_1^2 \omega_3^2} - \frac{\omega^4}{\omega_2^2 \omega_3^2} + \frac{\left(1 - k_{12}^2 - k_{23}^2\right)\omega^6}{\omega_1^2 \omega_2^2 \omega_3^2} - 1 \right)^2 + \frac{\omega^2}{Q^2 \omega_3^2} \left(\frac{\left(1 - k_{12}^2\right)\omega^4}{\omega_1^2 \omega_2^2} - \frac{\omega^2}{\omega_1^2} - \frac{\omega^2}{\omega_2^2} + 1 \right)^2}} \quad (3)$$

From Equation (3), it can be readily observed that if:

$$\frac{\left(1 - k_{12}^2\right)\omega^4}{\omega_1^2 \omega_2^2} - \frac{\omega^2}{\omega_1^2} - \frac{\omega^2}{\omega_2^2} + 1 = 0 \quad (4)$$

then the output current in Equation (3) can be rewritten as:

$$I_3 = \frac{\sqrt{C_1 C_3}\, k_{12} k_{23} \omega^5 V_{in}}{\omega_1 \omega_2^2 \omega_3 \left| \frac{\omega^2}{\omega_1^2} + \frac{\omega^2}{\omega_2^2} + \frac{\omega^2}{\omega_3^2} - \frac{\left(1 - k_{12}^2\right)\omega^4}{\omega_1^2 \omega_2^2} - \frac{\left(1 - k_{23}^2\right)\omega^4}{\omega_1^2 \omega_3^2} - \frac{\omega^4}{\omega_2^2 \omega_3^2} + \frac{\left(1 - k_{12}^2 - k_{23}^2\right)\omega^6}{\omega_1^2 \omega_2^2 \omega_3^2} - 1 \right|} \quad (5)$$

which is insensitive to Q. Due to the fact that Q is inversely proportional to R_L, I_3 in Equation (5) is insensitive to R_L. This load-independent output current is a very desirable feature in three-coil WPT system. This guarantees constant output current when the load changes without using control circuit.

By solving Equation (4), we can obtain the frequencies for load-independent output current in three-coil WPT. Because $1 - k_{12}^2 > 0$ holds, and the discriminant (*i.e.*, $\Delta = \left(\omega_1^2 - \omega_2^2\right)^2 + 4k_{12}^2 \omega_1^2 \omega_2^2$) in

Equation (4) is positive, according to Vieta's formulas, the bi-quadratic Equation (4) has two positive roots:

$$\omega = \left[\frac{\left(\omega_1^2 + \omega_2^2\right) \pm \sqrt{\left(\omega_1^2 - \omega_2^2\right)^2 + 4k_{12}^2\omega_1^2\omega_2^2}}{2\left(1 - k_{12}^2\right)} \right]^{0.5} \tag{6}$$

where the smaller one is ω_- and the larger one is ω_+.

Specifically, when the resonant frequencies of the coils are identical, that is, $\omega_1=\omega_2=\omega_3=\omega_0$, substituting $\omega_1=\omega_2=\omega_3=\omega_0$ into Equation (6), the frequencies for load-independent output current in a three-coil WPT in Equation (6) can be reduced as:

$$\omega = \frac{\omega_0}{\sqrt{1 \pm k_{12}}} \tag{7}$$

The expressions of the RMS of the currents in the TX, repeating coil, and RX (*i.e.*, I_1, I_2, and I_3) can be obtained by solving Equation (1). Thus, the transfer efficiency η in a three-coil WPT system is defined as the ratio of the power dissipation in the load and the total power supplied by the source [23–25]:

$$\eta = \frac{I_3^2 R_L}{I_1^2 R_1 + I_2^2 R_2 + I_3^2 \left(R_3 + R_L\right)} \tag{8}$$

The output power P_{out} in three-coil WPT system is calculated by:

$$P_{out} = I_3^2 R_L \tag{9}$$

Figures 3 and 4 show how the calculated output current varies with the operating frequency under three loading conditions in a three-coil WPT system with the parameters listed in Table 1. The coupling coefficients shown in Figure 3 are $k_{12} = 0.1$ and $k_{23} = 0.2$, and that in Figure 4 are $k_{12} = 0.5$ and $k_{23} = 0.4$.

Table 1. Parameters of the experimental setup.

Symbol	Note	Value
V_{in}	RMS source voltage	30 V
f_1, f_2, f_3	Resonant frequency of coil 1, 2, 3	105 kHz, 100 kHz, 95 kHz
L_1, L_2, L_3	Inductance of coil 1, 2, 3	58.91 uH, 37.25 uH, 50.12 uH
C_1, C_2, C_3	Capacitance of coil 1, 2, 3	39 nF, 68 nF, 56 nF
R_1, R_2, R_3	Resistance of coil 1, 2, 3	0.50 Ω, 0.39 Ω, 0.46 Ω
R_L	Load resistance	12 Ω, 18 Ω, 32 Ω

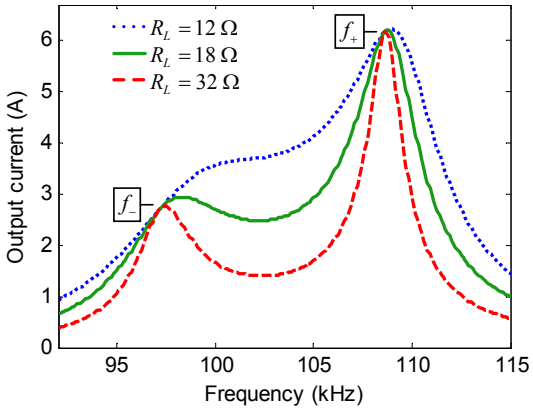

Figure 3. Calculated output current *versus* frequency in a three-coil WPT when $k_{12} = 0.1$ and $k_{23} = 0.2$.

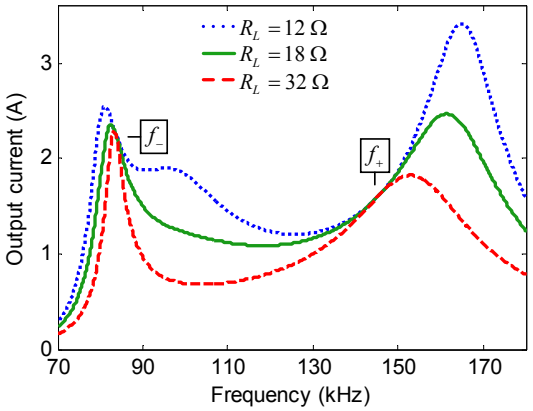

Figure 4. Calculated output current *versus* frequency in a three-coil WPT when $k_{12} = 0.5$ and $k_{23} = 0.4$.

As presented in Figures 3 and 4, for the given coupling coefficients k_{12} and k_{23}, there are two operating frequencies at which I_3 is irrelevant to R_L. In Figure 3, $f_- = \omega_-/2\pi = 97.15$ kHz and $f_+ = \omega_+/2\pi = 108.62$ kHz; in Figure 4, $f_- = \omega_-/2\pi = 83.57$ kHz and $f_+ = \omega_+/2\pi = 145.09$ kHz.

4. Experiments

To verify the above analysis for a three-coil WPT, an experimental setup is implemented, and a set of experiments are performed. Three polypropylene capacitor with the capacitance value 39 nF, 56 nF, and 68 nF are used as the external capacitors. The three-coil WPT system is composed of three circular coils with a radius of 100 mm. These coils are fabricated with Litz wire, and the radius of the Litz wire used in the TX, the repeating coil, and the RX are 1.3 mm, 1.3 mm, and 1.0 mm, respectively. The turn number of the Litz wire used in the TX, the repeating coil, and the RX are 10, 8, and 9, respectively. The inductance of each coil can be measured by an LCR meter. Figure 1 displays the photograph of the experimental setup, whose parameters are listed in Table 1. Standard sinusoidal signals generated by a signal generator are amplified by a power amplifier and fed to the transmitting coil of the three-coil WPT system.

For two coaxial circular coils, the mutual inductance can be calculated using Equation (10) [25,26]

$$M = \mu_0 N_1 N_2 \sqrt{r_1 r_2}\left[\left(\frac{2}{\gamma}-\gamma\right)K(\gamma)-\frac{2}{\gamma}E(\gamma)\right] \tag{10}$$

where $\gamma = \sqrt{4r_1r_2/\left((r_1+r_2)^2+d^2\right)}$, $K(\gamma)$ and $E(\gamma)$ are complete elliptic integrals of the first and second kind, respectively, and the values of $K(\gamma)$ and $E(\gamma)$ can be obtained by Sidhu's method, as elucidated in [27]; μ_0 is the permeability of vacuum, N_1 and N_2 are the number of turns of the two coils, r_1 and r_2 are the radius of coil-1 and coil-2, respectively, and d is the distance between the two coils.

The inductances of the coils are measured by an LCR meter, and the mutual inductance between the coils is calculated by Equation (10); thus, the coupling coefficients can be calculated by Equation (2).

Figures 5 and 6 show the measured output current *versus* the operating frequency under three loading conditions in a three-coil WPT.

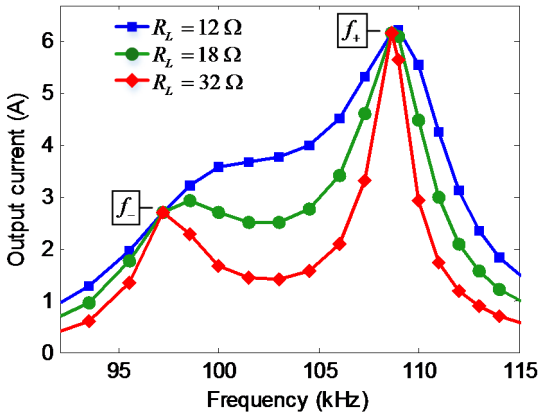

Figure 5. Measured output current *versus* frequency in a three-coil WPT when $k_{12} = 0.1$ and $k_{23} = 0.2$.

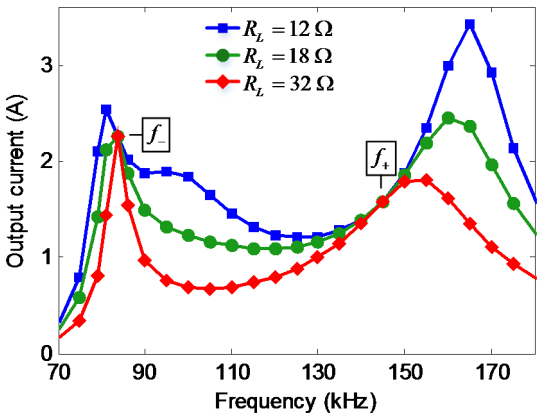

Figure 6. Measured output current *versus* frequency in a three-coil WPT when $k_{12} = 0.5$ and $k_{23} = 0.4$.

As shown in Figure 5, when $k_{12} = 0.1$ and $k_{23} = 0.2$, there are two operating frequencies, *i.e.*, $f_- = 97.3$ kHz and $f_+ = 108.5$ kHz, at which I_3 is insensitive to R_L; these findings are consistent with the calculated results in Figure 3.

In Figure 6, when $k_{12}=0.5$ and $k_{23}=0.4$, the frequencies for load-independent output current are $f_{-}=83.7$ kHz and $f_{+}=145.0$ kHz, which agree with the calculated results in Figure 4.

Upon comparing the trend of the output current in Figures 5 and 6 with that in Figures 3 and 4, respectively, the measured results confirm the calculated results.

Furthermore, Equation (6) demonstrates that the frequency for load-independent output current is a function of the coupling coefficient k_{12} and irrelevant to k_{23}, that is, when k_{12} is given, the frequencies for load-independent output current in a three-coil WPT are determined.

Figure 7 presents the calculated and measured frequencies for load-independent output current *versus* the coupling coefficient k_{12} in a three-coil WPT. The dotted line and dashed line are the calculated values of f_{-} and f_{+}, respectively. The points are measured data: the circles and diamonds denote f_{-} and f_{+}, respectively. The calculated and measured results are in good agreement, which validates the conclusion reached in Section 3.

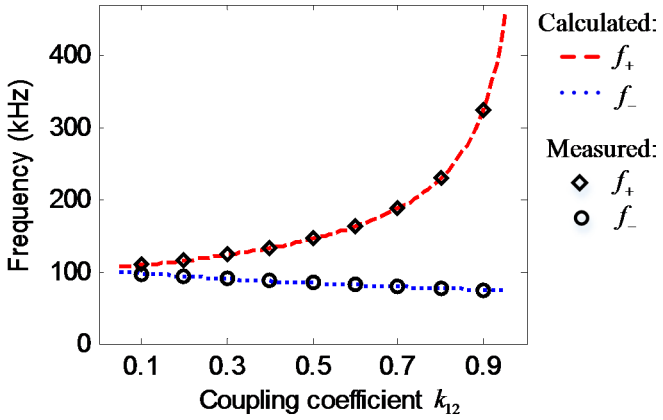

Figure 7. Calculated and measured frequencies for load-independent output current *versus* coupling coefficient k_{12} in a three-coil WPT.

When $k_{12}=0.1$ and $k_{23}=0.2$, the measured results of output power and transfer efficiency *versus* frequency in a three-coil WPT system are displayed in Figure 8a,b, respectively. When $k_{12}=0.5$ and $k_{23}=0.4$, Figure 9a,b reveal how the measured output power and transfer efficiency vary with frequency in a three-coil WPT system, respectively.

As shown in Figure 8a, in the case of the small coupling coefficients (*i.e.*, at long distances), when the load resistance is relatively small, there is only peak value of the output power; when the load resistance grows, that is, the quality factor decreases, two peaks of the output power arise because of the frequency splitting [23]. Figure 9a indicates that when the coupling coefficients are relatively large (*i.e.*, at close distances), there are two peak values of the output power, which is called the frequency splitting phenomenon [23].

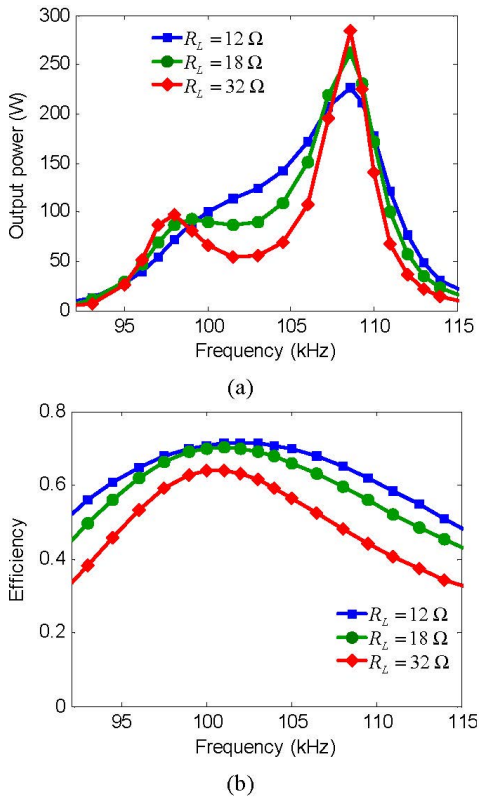

Figure 8. Measured results *versus* frequency in a three-coil WPT when $k_{12} = 0.1$ and $k_{23} = 0.2$: (**a**) output power; and (**b**) efficiency.

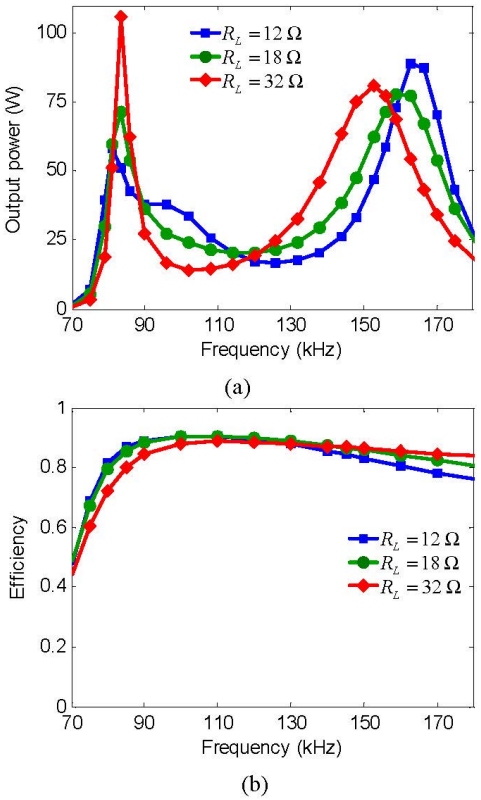

Figure 9. Measured results *versus* frequency in a three-coil WPT when $k_{12} = 0.5$ and $k_{23} = 0.4$: (**a**) output power; and (**b**) efficiency.

When the load resistance varies, the transfer efficiency in the three-coil WPT system varies accordingly, that is, there exists an optimal load to obtain the maximal transfer efficiency. Comparing Figure 8b with Figure 9b, we observe that increasing the coupling coefficients (*i.e.*, at close distances) results in higher transfer efficiency.

5. Conclusions

Based on circuit theory, load-independent output current in a three-coil WPT system is thoroughly studied. By introducing six factors, namely, the coupling coefficients (k_{12} and k_{23}), the quality factor (Q), and the resonant frequency of each coil (ω_1, ω_2, and ω_3), and substituting these factors into the expression of the RMS of the output current, we propose an intuitive method of calculating the frequency for load-independent output current, which indicates that there are two frequencies that can achieve load-independent output current in three-coil WPT. An experimental setup is implemented, and the measured results show excellent agreement with the theoretical analysis. Furthermore, the measured results of output power and transfer efficiency in a three-coil WPT system are also presented.

In comparison with previous study [18], this study can assist us in achieving a load-independent output current at longer distances. The proposed method and conclusion provide guidelines for selecting the optimal operating frequency in three-coil WPT system to obtain a constant output current under varying load conditions, which is a significant progress toward practical applications for WPT technology.

Acknowledgments

This work was supported by the National Natural Science Foundation of China (51277120).

Author Contributions

Longzhao Sun proposed the main idea, performed the experiments, and wrote the manuscript. Houjun Tang contributed to the discussion of this study. Yingyi Zhang double-checked the results and the whole manuscript. All authors have approved the final version of this manuscript.

Conflicts of Interest

The authors declare no conflict of interest.

References

1. Chen, Q.; Wong, S.C.; Tse, C.K.; Ruan, X. Analysis, design, and control of a transcutaneous power regulator for artificial hearts. *IEEE Trans. Biomed. Circuits Syst.* **2009**, *3*, 23–31.
2. Ahn, D.; Hong, S. Wireless power transmission with self-regulated output voltage for biomedical implant. *IEEE Trans. Ind. Electron.* **2014**, *61*, 2225–2235.
3. Nair, V.V.; Choi, J.R. An integrated chip high-voltage power receiver for wireless biomedical implants. *Energies* **2015**, *8*, 5467–5487.
4. Ho, J.S.; Kim, S.; Poon, A.S.Y. Midfield wireless powering for implantable systems. *IEEE Proc.* **2013**, *101*, 1369–1378.

5. Zhong, W.X.; Liu, X.; Hui, S.R. A novel single-layer winding array and receiver coil structure for contactless battery charging systems with free-positioning and localized charging features. *IEEE Trans. Ind. Electron.* **2011**, *58*, 4136–4144.
6. Hui, S.Y. Planar wireless charging technology for portable electronic products and Qi. *IEEE Proc.* **2013**, *101*, 1290–1301.
7. Cheng, S.J.; Chiu, H.J.; Lo, Y.K.; Kuo, S.W.; Jen, K.K.; Fu, K.S.; You, G.H.; Chen, K.F.; Kao, C.M. Design and implementation of a contact-less power charger for robot applications. *Int. J. Circuit Theory Appl.* **2014**, *42*, 584–604.
8. Zhang, Z.; Chau, K.T.; Liu, C.; Qiu, C.; Ching, T.W. A positioning-tolerant wireless charging system for roadway-powered electric vehicles. *J. Appl. Phys.* **2015**, *117*, 17B520, doi:10.1063/1.4916187.
9. Zhang, Z.; Chau, K.T.; Liu, C.; Qiu, C.; Lin, F. An efficient wireless power transfer system with security considerations for electric vehicle applications. *J. Appl. Phys.* **2014**, *115*, 17A328, doi:10.1063/1.4866238.
10. Covic, G.A.; Boys, J.T. Modern trends in inductive power transfer for transportation applications. *IEEE J. Emerg. Sel. Top. Power Electron.* **2013**, *1*, 28–41.
11. Li, W.; Mi, C.C.; Li, S.; Deng, J.; Kan, T.; Zhao, H. Integrated LCC compensation topology for wireless charger in electric and plug-in electric vehicles. *IEEE Trans. Ind. Electron.* **2015**, *62*, 4215–4225.
12. Zierhofer, C.M.; Hochmair, E.S. High-efficiency coupling insensitive transcutaneous power and data transmission via an inductive link. *IEEE Trans. Biomed. Eng.* **1990**, *37*, 716–722.
13. Baker, M.W.; Sarpeshkar, R. Feedback analysis and design of RF power links for low-power bionic systems. *IEEE Trans. Biomed. Circuits Syst.* **2007**, *1*, 28–38.
14. Villa, J.; Sallan, J.; Osorio, J.; Llombart, A. High-misalignment tolerant compensation topology for ICPT systems. *IEEE Trans. Ind. Electron.* **2012**, *59*, 945–951.
15. Zierhofer, C.M.; Hochmair, E.S. The class-E concept for efficient wide-band coupling-insensitive transdermal power and data transfer. *IEEE Proc. Annu. Int. Conf.* **1992**, *2*, 382–383.
16. Zhang, W.; Wong, S.C.; Tse, C.K.; Chen, Q. Design for efficiency optimization and voltage controllability of series–series compensated inductive power transfer systems. *IEEE Trans. Power Electron.* **2014**, *29*, 191–200.
17. Zhang, W.; Wong, S.C.; Tse, C.K.; Chen, Q. Analysis and comparison of secondary series- and parallel-compensated inductive power transfer systems operating for optimal efficiency and load-independent voltage-transfer ratio. *IEEE Trans. Power Electron.* **2014**, *29*, 2979–2990.
18. Zhang, W.; Wong, S.C.; Tse, C.K.; Chen, Q. Load-independent duality of current and voltage outputs of a series- or parallel-compensated inductive power transfer converter with optimized efficiency. *IEEE J. Emerg. Sel. Top. Power Electron.* **2015**, *3*, 137–146.
19. Pinuela, M.; Yates, D.C.; Lucyszyn, S.; Mitcheson, P.D. Maximizing DC-to-load efficiency for inductive power transfer. *IEEE Trans. Power Electron.* **2013**, *28*, 2437–2447.
20. Puccetti, G.; Reggiani, U.; Sandrolini, L. Experimental analysis of wireless power transmission with spiral resonators. *Energies* **2013**, *6*, 5887–5896.
21. Wei, X.; Wang, Z.; Dai, H. A critical review of wireless power transfer via strongly coupled magnetic resonances. *Energies* **2014**, *7*, 4316–4341.

22. Kiani, M.; Ghovanloo, M. The circuit theory behind coupled-mode magnetic resonance-based wireless power transmission. *IEEE Trans. Circuits Syst. Part I Regul. Pap.* **2012**, *59*, 2065–2074.
23. Ahn, D.; Hong, S. A study on magnetic field repeater in wireless power transfer. *IEEE Trans. Ind. Electron*. **2013**, *60*, 360–371.
24. Zhang, Y.; Zhao, Z.; Lu, T. Quantitative analysis of system efficiency and output power of four-coil resonant wireless power transfer. *IEEE J. Emerg. Sel. Top. Power Electron.* **2015**, *3*, 184–190.
25. Lee, S.H.; Lorenz, R.D. Development and validation of model for 95% efficiency 220 W wireless power transfer over a 30-cm air gap. *IEEE Trans. Ind. Appl.* **2011**, *47*, 2495–2504.
26. Zhang, X.; Ho, S.L.; Fu, W.N. Quantitative design and analysis of relay resonators in wireless power transfer system. *IEEE Trans. Magn.* **2012**, *48*, 4026–4029.
27. Miller, H.C. Inductance formula for a single-layer coil. *IEEE Proc.* **1987**, *75*, 256–257.